# Neutrino-nucleus quasi-elastic and 2p2h interactions up to 10 GeV

R. Gran,[1] J. Nieves,[2] F. Sanchez,[3] and M. J. Vicente Vacas[2]

[1]*Department of Physics, University of Minnesota – Duluth, Duluth, Minnesota 55812, USA*
[2]*Instituto de Física Corpuscular (IFIC), Centro Mixto CSIC-Universidad de Valencia,*
*Institutos de Investigación de Paterna, Apartado 22085, E-46071, Valencia, Spain*
[3]*Institut de Fisica d'Altes Energies (IFAE), Bellaterra, Barcelona, Spain*
(Dated: February 17, 2014)

We extend to 10 GeV results from a microscopic calculation of charged-current neutrino-nucleus reactions that do not produce a pion in the final state. For the class of events coming from neutrino interactions with two nucleons producing two holes (2p2h), limiting the calculation to three-momentum transfers less than 1.2 GeV produces a two-dimensional distribution in momentum and energy transfer that is roughly constant as a function of energy. The cross section for 2p2h interactions approximately scales with the number of nucleons for isoscalar nuclei, similar to the quasi-elastic cross section. When limited to momentum transfers below 1.2 GeV, the cross section is 26% of the quasi-elastic cross section at 3 GeV, but 14% if we neglect a $\Delta_{1232}$ resonance absorption component. The same quantities are 33% and 17% for antineutrinos. For the quasi-elastic interactions, the full nuclear model with long range correlations produces an even larger, but approximately constant distortion of the shape of the four-momentum transfer at all energies above 2 GeV. The 2p2h enhancement and long-range correlation distortions to the cross section for these interactions are significant enough they should be observable in precision experiments to measure neutrino oscillations and neutrino interactions at these energies, but also balance out and produce less total distortion than each effect does individually.

## I. INTRODUCTION

Neutrino interactions in nuclei at energies up to 10 GeV are the core of current and upcoming neutrino experiments to measure oscillation effects, neutrino interaction cross sections, and to search for new physics beyond the standard model. The precision of these experiments will be limited by systematic uncertainties, likely including those from neutrino interaction modeling. The on-axis NuMI flux has modes that peak near 3 GeV or 6 GeV and serve MINOS and MINERvA with a similar 3 GeV design proposed for LBNE. The off-axis flux from the same beam as used by NOvA peaks at 2 GeV and is tuned to include the energy of the expected maximum oscillation probability. Even low energy experiments like T2K have a high energy tail, and MicroBooNE will have a secondary peak at 2 GeV neutrino energy from off-axis kaon decay neutrinos from the nearby NuMI beamline.

Measuring and modeling neutrino-nucleus interactions has recently improved because of the effort surrounding especially the MiniBooNE double-differential quasi-elastic (QE) data [1]. Those data peak near 600 MeV neutrino energy. Several groups are investigating better models of the nuclear environment described in the review article [2], especially the use of the random phase approximation (RPA) to compute the effects of long-range nucleon-nucleon correlations affecting the QE and $\Delta_{1232}$ interactions. Computing the RPA series requires a model for the effective (N and $\Delta_{1232}$) baryon-baryon interaction in the nuclear medium, including short-range correlations (SRC). Also, a new class of interactions is now being computed where the reaction involves two or three nucleons and producing two or three holes in the nucleus (2p2h and 3p3h). These components are required to describe existing electron scattering data, and we find that they are also significant for neutrino interactions [3–10].

In this paper we present results from our microscopic model for charged-current interactions that do not produce a pion in the final state, now limited at 10 GeV and three-momentum transfer of 1.2 GeV, the first detailed calculation of this type at these energies. Previously computed results [6–8] for energies below 1.5 GeV compare well with MiniBooNE data and independent calculations by another group [3, 4]. In this paper, these new calculations are also compared to other predictions obtained empirically from electron scattering data and a brief interpretation of existing data is included as well.

## II. STRUCTURE OF THE CALCULATION

The high energy results presented here are the extension of a long-standing program to build up a complete microscopic calculation of the neutrino-nucleus cross section [6, 11–13] which historically comes from work at neutrino energy around 150 MeV [14].

The QE process uses a local Fermi gas (LFG) which includes Pauli blocking, Fermi motion, removal energy, and Coulomb distortion. Most significantly, long and short range nucleon-nucleon correlations are included using the random phase approximation (RPA) approach that accounts for both nucleon-hole and $\Delta_{1232}$-hole components [11]. The free nucleon form factors are the stan-
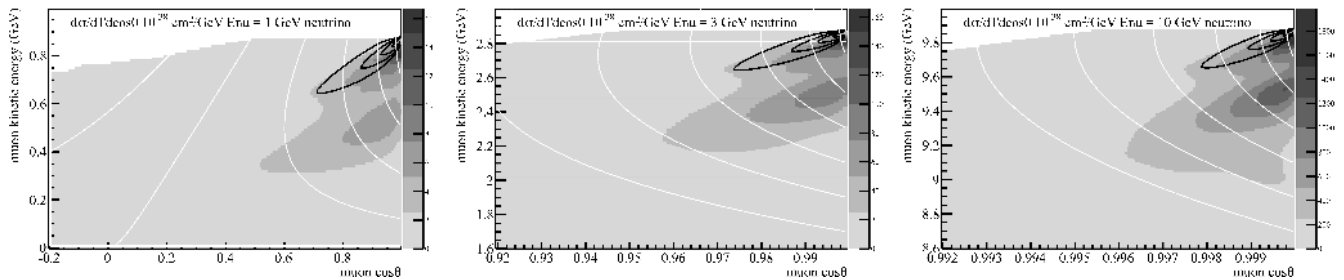
FIG. 1. Double differential 2p2h cross section $d\sigma/dT_\mu dcos\theta_\mu$ ($10^{-38}$ cm$^2$/GeV) for neutrino-carbon interactions at energies of 1.0, 3.0, and 10.0 GeV. The black contours show the location of the QE events with four equally spaced contours from zero to maximum (which varies among the plots) and has a width due to the nuclear model. The white shows lines of constant three-momentum transfer from 0.2 to 1.2 GeV.

dard ones with an axial mass $M_A = 1.0$ GeV (different from [7, 14]) used in a dipole axial form factor and vector form factors from [15]. In the results that follow we also show a comparison of these calculations to the same free nucleon cross section applied within the local Fermi gas nucleus but without RPA effects (noRPA) which gives results within $\pm 5\%$ of the default QE cross section of the GENIE 2.8.0 neutrino event generator [16] used by many experiments. The differences can be attributed to the choice of the axial mass parameter, vector form factors and the use of the global Fermi gas in GENIE instead of a local Fermi gas in Ref. [11].

The non-QE component presented here is constructed from a many body expansion of modes where the exchanged W boson is absorbed by two or three nucleons. We refer to this set of processes generically as two-particle two-hole channels (2p2h) which are also called meson exchange currents. The details are described in [6–8] The equivalent component for inclusive electron-nucleus scattering fills in the so-called "dip region" between the QE and $\Delta$ peaks [17], and plays the same role here in neutrino-nucleus scattering. The calculation includes processes that do not have a pion or an on-shell $\Delta$ in the diagram-level final state, and so are "QE-like" by some experimental definitions.

One class of 2p2h processes have $\Delta$ kinematics in which a $\Delta N \rightarrow NN$ absorption process occurs. Some contemporary event generators include pionless processes with $\Delta$ kinematics using a $\Delta$ absorption process or a pion absorption with a final state interaction (FSI) cascade rescattering model, or both. We can separate the pieces of the calculation to not include the $\Delta$ absorption process, in doing so approximately illustrate the size of the modification relative to current neutrino interaction generator codes. This is done by subtracting the $\Delta$ absorption cross section, so interference terms between the $\Delta$ resonance excitation mechanism and non-$\Delta$ components are kept.

These calculations are made with no parameters tuned to neutrino-nucleus data except for the choice of $M_A = 1.0$ GeV for the axial form factor, which is essentially tuned to deuterium bubble chamber data.

In previous work with neutrino energies below 1.5 GeV,

the entire kinematic space was well described by the model and its calculations. As the neutrino energy increases, it opens up a region of high momentum and energy transfer in the kinematics. The model does not include 2p2h production via resonances beyond the $\Delta$ or related interference terms. Also, as the computation is configured, the result is not adequately accurate for high three-momentum transfers. For both reasons, the 2p2h computation is not suited to describe this high momentum-transfer region of kinematic space.

The low three-momentum transfer part of the calculation still remains as accurate as it is at low neutrino energies, and includes most of the cross section and the most interesting structure. In addition, experimental analysis of charged current muon and antimuon samples with low hadron multiplicity are often restricted to the forward direction due to detector geometry design. Higher momentum transfer events exit the detectors out the side and are reconstructed with poor resolution or cut completely. The calculation we present here is well suited to the most relevant energies and regions of kinematic acceptance for current experiments.

## III. RESULTS

The three plots in Fig. 1 show the neutrino-carbon 2p2h cross section in the muon experimental observables at energies of 1.0, 3.0, and 10.0 GeV. The bounds of each plot are constructed so they contain events up to and a little beyond three-momentum transfer of 1.2 GeV. The gray scale gives the 2p2h double-differential cross section in units of $10^{-38}$ cm$^2$/GeV. Clearly evident is an upper nondelta band and the lower $\Delta$ component. Because we restrict the calculation to the nonresonant and $\Delta$ components, higher resonance RN$\rightarrow$NN transitions (or their interference effects) do not appear below the delta band. Two sets of contours are overlaid on the plot: the black contours are from the QE calculation; the white contours are lines of constant three-momentum transfer up to 1.2 (in steps of 0.2) GeV. Lines of constant energy transfer can be inferred from the vertical axis.

As a function of energy, the structure and magnitude of the 2p2h cross sections are quite stable. In Table I, we show the integral of the QE and 2p2h cross sections within the three-momentum transfer $q_3 < 1.2$ GeV contour. In addition, the total QE cross section is also given for carbon. The computed QE cross section decreases slowly with energy following the inherent dependence of the free-nucleon cross section. The 2p2h estimates are slowly increasing primarily because the calculation is adding more cross section below the $\Delta$ near the right axis. With the $\Delta$ component, the 2p2h cross section is 26% of the total QE cross section, without the $\Delta$ absorption component it is 14% for 3.0 GeV neutrino interactions, and rises to 32% and 17% at 10 GeV respectively.

## A. Momentum and energy transfer 2D plane

These cross sections are naturally better expressed in terms of momentum and energy transfer, so the three plots shown above can be summarized as in Fig. 2. In these kinematics, the $\Delta$ component is the top peak, and the non-$\Delta$ part peaks lower, just above the QE kinematics and fills in the dip region. As mentioned above, the $\Delta$ component peak could be mostly assimilated to the $\Delta N \rightarrow NN$ absorption process; it is the production of an on-shell $\Delta$, subsequently reabsorbed by another nucleon. Such contribution is often not included in what is commonly called a meson-exchange current. In the energy range from 2.0 to 10.0 GeV, the cross section in and surrounding the two peaks stays within 10% of the value shown here, because the hadronic tensor does not change and the leptonic part of the calculation changes slowly. In the tails of the distribution, especially along diagonal $q_0 = q_3$ edge, the differences grow to 30% with higher energy.

Both parts of the 2p2h cross section appear in a different location than the QE part of the cross section. Rather than being near $W_\Delta = 1.232$ GeV or nucleon $W \approx 0.938$ MeV, the non-$\Delta$ component peaks near a line of $W \approx 1.00$ GeV ($W^2 = M_N^2 + 2M_N q_0 + q^2$) at very-low $-q^2 = Q^2 < 0.5$ GeV$^2$ with a substantial asymmetric tail toward the $\Delta$ and higher energy transfer. At higher $Q^2$ the 2p2h peak crosses under the QE line but retains the asymmetric tail. In all cases, the 2p2h contribution is wider than the QE and effectively fills in the QE and $\Delta$ and the dip region between them. The $\Delta$ absorption component peaks at $W = 1.232$ GeV as expected.

An experiment that classifies these as QE-like, because no pion was observed and/or because the proton was below the reconstruction threshold, might choose to use the QE lepton kinematics to reconstruct the neutrino energy. See, for example, the discussion in [13]. Though the QE events will be unbiased up to the average removal energy estimate, most of the 2p2h nondelta component will pick up a bias which is typically 100 MeV below the true neutrino energy while the $\Delta$ component will be centered 350 MeV low. These estimates are constant with neutrino en-
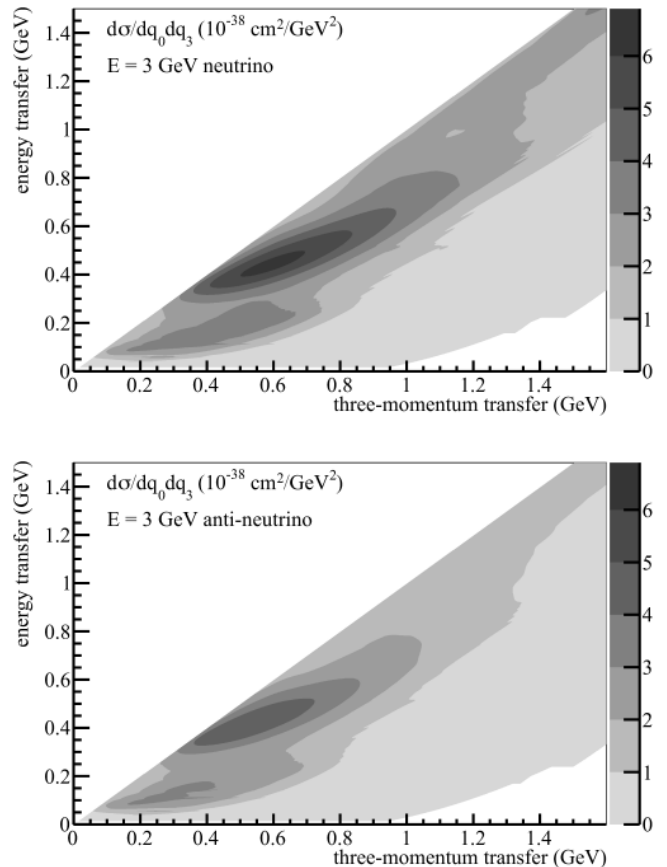


FIG. 2. The 2p2h cross section $d\sigma/dq_0dq_3$ vs. energy transfer and three-momentum transfer for 3.0 GeV neutrinos (top) and antineutrinos (bottom).

ergy, so they become a smaller fractional bias as neutrino energy increases. Likewise, if the biased energy estimate is then used to make an estimate of the reconstructed $Q^2$, that too will be biased low.

**Antineutrino case** All the trends for the antineutrino case are similar to the neutrino case, and are included in Fig. 2 and Table I. The 2p2h components of the antineutrino case rise similar to the underlying QE antineutrino cross section and are 33% and 19% with and without the $\Delta$ absorption component at 3 GeV, relative to the QE+RPA cross section. This is a somewhat higher fraction relative to the QE rate than the neutrino version, and also the QE with and without RPA are themselves 9% different at 3 GeV, converging as energy rises.

**Application to event generators** The distinction between the 2p2h cross sections with and without the $\Delta$ component is important. A portion of the cross section involving a $\Delta$, corresponding specifically to $\Delta$ absorption, can be incorporated into a modern event generator via its treatment of $\Delta$ and/or pion final state reinteractions in the nucleus. Simply adding the full cross section presented here could double-count some of these events, so Table I also gives the cross section without $\Delta$ absorp-

TABLE I. The 2p2h cross section in carbon vs. energy. The contribution saturates as a function of three-momentum transfer to a value that is 29% of the QE cross section for neutrino, 32% for antineutrino, an estimate for the nondelta component without the $\Delta$ absorption component is 15% and 17% of the QE cross section for neutrino and antineutrino.

| Energy (GeV) | whole cross section (x $10^{-38}$ cm$^2$) | | | three-momentum transfer < 1.2 GeV | | |
| | QE LFG+RPA | QE LFG noRPA | 2p2h | 2p2h no $\Delta$ | QE LFG+RPA | QE LFG noRPA |
| --- | --- | --- | --- | --- | --- | --- |
| 1 $\nu_\mu$ | 5.61 | 5.66 | 1.27 | 0.563 | 5.20 | 5.36 |
| 2 | 5.65 | 5.61 | 1.41 | 0.704 | 4.52 | 4.74 |
| 3 | 5.45 | 5.45 | 1.43 | 0.735 | 4.30 | 4.54 |
| 5 | 5.22 | 5.25 | 1.46 | 0.761 | 4.14 | 4.39 |
| 10 | 5.04 | 5.10 | 1.47 | 0.781 | 4.01 | 4.27 |
| 1 $\overline{\nu}_\mu$ | 1.56 | 1.96 | 0.459 | 0.306 | 1.56 | 1.95 |
| 2 | 2.68 | 3.03 | 0.887 | 0.520 | 2.52 | 2.89 |
| 3 | 3.26 | 3.55 | 1.07 | 0.609 | 2.93 | 3.27 |
| 5 | 3.83 | 4.05 | 1.24 | 0.686 | 3.29 | 3.61 |
| 10 | 4.31 | 4.47 | 1.38 | 0.749 | 3.58 | 3.88 |

tion. The alternative approximation is to discard events from an event generator where a $\Delta$ was absorbed and keep the whole pionless cross section estimate described here.

**Uncertainty on the calculations** Though the prediction for the cross section within a choice of three-momentum cutoff is stable, and the differential cross section itself is small, a substantial amount of cross section is not included in the integration because of the large kinematic space. Moving the cutoff value back to 1.1 GeV or forward to 1.3 GeV reduces or increases the integrated cross section by about 10%, or about 8% for the component without the $\Delta$.

The above variations occur without including higher resonances. As the neutrino energy increases, the second resonance region of nucleon excitations ($P_{11}(1440)$, $D_{13}(1520)$ and $S_{11}(1535)$), followed by absorption on another nucleon, might play some role at high energy transfers, above $q_0 > 0.9-1$ GeV (note that $q^2 < 0$ and hence $q_3$ is always bigger than $q_0$). According to Refs. [18, 19], the $N(1520)$ resonance would be the only one whose effects might not be totally negligible, at least for neutrino energies below 2 GeV. But even this latter $N^*$ contribution represents only a quite small fraction of that of the $\Delta$. The results shown in Fig. 5.11 of [19] illustrate this especially well. There, the integrated cross section for CC induced resonance production on the proton and on the neutron are displayed. Nevertheless, this source of uncertainty might contribute an additional 10% to the high momentum transfer part of the calculation. However, the cross section involving higher resonances (neglecting interference contributions) is already incorporated into most of the modern event generators, as mentioned in the paragraph above for the case of the $\Delta$, the issue is how much migrates to a QE-like final state because of in-medium absorption of the resonance state. Because of the dominance of the $\Delta$, and the important modifications of its properties inside of a nuclear medium, we have prioritized its contribution, together with that of the non-resonant background terms *and* the quantum mechanical
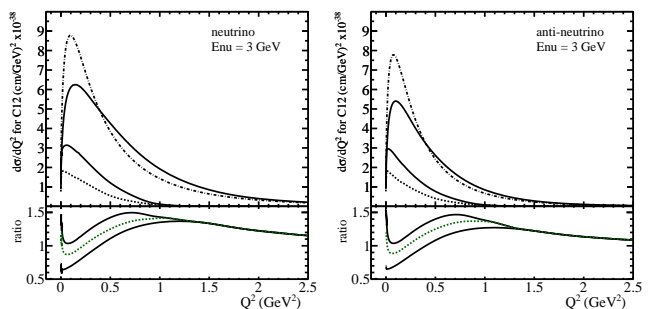


FIG. 3. The $Q^2$ distributions for QE and 2p2h contributions, neutrino case (left) and antineutrino (right) for incoming energy of 3 GeV. The QE and 2p2h cross sections are the solid upper and solid lower lines respectively. Upper dashed line is the QE without RPA; lower dashed line is the 2p2h cross section without the $\Delta$ absorption component. The lower solid ratio line is $QE_{full}/QE_{noRPA}$, the dashed ratio line is $(QE_{full} + 2p2h_{no\Delta})/QE_{noRPA}$, and the upper ratio line is $(QE_{full} + 2p2h_{with\Delta})/QE_{noRPA}$. For all variations, the QE lines are the complete cross section but the 2p2h lines truncate the integration at $q_3 = 1.2$ GeV, causing it to also not contribute to the ratio above $Q^2 = 1.2$.

interferences among all of possible mechanisms, a combination that is usually not considered in the neutrino interaction event generators.

### B. Four momentum transfer distributions

Integrating the cross section in the previous figures along lines of $Q^2$ gives Fig. 3. The solid lines are from the calculation described above; the top solid one is the full QE model with local Fermi gas and nucleon correlation effects, the bottom one is the full 2p2h contribution. The dashed lines are special versions for comparison. The top is QE without RPA, similar to the standard treatment for neutrino experiments. The bottom dashed line is the 2p2h contribution without the delta absorption compo-

nent. The QE components show the full cross section, integrated all the way to the end of the appropriate $Q^2$ contour. The integration for the 2p2h contribution is stopped at the three-momentum $q_3 = 1.2$ GeV boundary, like the values in Table I.

The bottom portion of each figure shows two ratios. The lower solid curve is the ratio of the full QE model to QE without RPA. The dashed curve is the ratio of ( $QE_{full}$+ 2p2h$_{no\Delta}$) / $QE_{noRPA}$, and the top solid curve is like the dashed curve but with the 2p2h $\Delta$ absorption component.

The 2p2h model contributes events at lower $Q^2$, and especially modifies the total for $Q^2 < 0.2$ GeV$^2$ where the QE rate is reduced due to Pauli blocking and RPA effects. Through the middle of the $Q^2$ region, it causes a mild shape distortion. For comparison to experimental results, the reconstructed $Q^2$ distribution will be further distorted, a little bit if calorimetry is available to estimate the neutrino energy, and a larger amount if the QE assumption and lepton kinematics are used. For the neutrino case, 2p2h interactions will be reconstructed low due a biased low $E_\nu$ estimate. At 3 GeV, this migration causes the reco version of the 2p2h cross section in Fig. 3 would be 20% higher near $Q^2 = 0$ and 20% lower near $Q^2 = 1$ GeV$^2$; at 10 GeV the effect is one-quarter this size. The bias due to calorimetry or two-particle kinematic reconstruction is more difficult to assess without explicit final state nucleons and final state reinteractions, which are beyond the scope of this paper. If they are put in a sample and reconstructed as if they are QE, the expectation is neutrino QE has energy deposits from a proton in the final state while 2p2h have a mix of $pn$ and $pp$, so the 2p2h component will have more missing energy. For antineutrino events, the 2p2h component mix of $pn$ and $nn$ will more often appear to have protonlike energy than expected for a pure QE sample with its neutron final state.

For experiments that are sensitive to the shape of the $Q^2$ distribution of a QE-like signal, the inclusion of nucleon-nucleon correlation effects in the RPA series yields a much larger shape distortion toward relatively more high-$Q^2$ interactions, with the 2p2h component filling in the suppression at very low $Q^2$. Correlation effects in this model are tuned to low energy nuclear phenomena, such as electron scattering and muon capture on nuclei, where they are essential for a good description of data [11]. The suppression to a factor of 0.6 at $Q^2 = 0$ is the same kinematics, and is the most robust part of this calculation. The point near $Q^2 = 0.4$ GeV$^2$ where the effect changes from suppression to enhancement is also where the tuning of correlation effects is well constrained [17]. In the calculation, the RPA effects go to 1.0 at very large $Q^2$ because sizes larger than one nucleon are no longer being probed. Technically, there should be a transition to probing neutrino-quark scattering which is not part of this calculation.

The low $Q^2$ suppression is a combination of both short and long range correlation effects. The trend moving toward $Q^2 = 1.1$ GeV$^2$ is an enhancement of the cross section but leaves the region where the model was tuned to other nuclear effect data, and this specific part is not relativistic, hence the model suffers from larger uncertainties. The maximum enhancement is 35% for the neutrino case and 25% for antineutrinos within our approach. These numbers should be taken with caution, since the model has been extracted beyond its reliable range. An alternate version of the calculation which has a covariant form and a 20% lower cross section at 1.1 GeV$^2$ roughly indicates the size of the uncertainty, though should not be considered a one-sigma statement. It is reasonable to expect some enhancement due to RPA above $Q^2 = 0.5$ GeV$^2$, before RPA effects become negligible. This feature is driven toward enhancement by the transverse part of the ph-ph interaction (second term in Eq. (36) of [11]) when it and also the longitudinal term both change sign. As the momentum transfer increases, the non-relativistic form of the first term in brackets and the simplification of g'(q) = g' = 0.63, which neglects the mild q dependence, contribute to uncertainty in the maximum size of the enhancement and how fast it drops to zero.

This higher $Q^2$ region is where the short range correlation (SRC) effects are most important. The model parameters are not specifically tuned to the equivalent electron scattering data, which also show an excess of cross section strength when SRC are not accounted for. A substantial SRC component in electron scattering is needed to reproduce for the tail of the measured nucleon momentum distribution and an enhancement of the cross section in kinematic regions away from where 2p2h and FSI contributions play a significant role. A recent and comprehensive review in electron scattering is provided by [20]. Another review [21] covers the SRC portion but also emphasizes a phenomenological connection with the EMC effect in deep inelastic scattering. Because we expect the 2p2h contribution to be small at these values of $Q^2$, neutrino scattering data with excellent coverage of the $Q^2 = 1$ GeV$^2$ region may also be an interesting new window to understanding this feature of the nuclear environment, and we include some discussion in a later section.

Not shown in these plots, the distortion as a function of $Q^2$ for all energies above 2 GeV is essentially constant. Compared to the 3 GeV calculation shown, it remains within 5% at all $Q^2$ away from the backscatter limit. The antineutrino case is similar, though the enhancement at high $Q^2$ is slightly less pronounced and as shown in Table I the resulting genuine cross section remains around 4% lower than the model without RPA, even at 10 GeV.

## C. Isospin content of the initial state

The 2p2h calculation yields 67% of the cross section coming from $pn$ pairs in the nucleus, for neutrino energy of 3 GeV, when the cross section is integrated to $q_3 = 1.2$ GeV. Part of this is from the $\Delta$ absorption

component which is explicitly given an initial state $pn$ fraction of 5/6. The portion of the 2p2h cross section not from $\Delta$ absorption (including the interference term) has only a 50% fraction coming from an initial $pn$ state. These results hold for the charged-current neutrino case $W^+ + np \rightarrow pp$ shown in Fig. 4 and also for the antineutrino $W^- + np \rightarrow nn$. The isospin content is not uniform
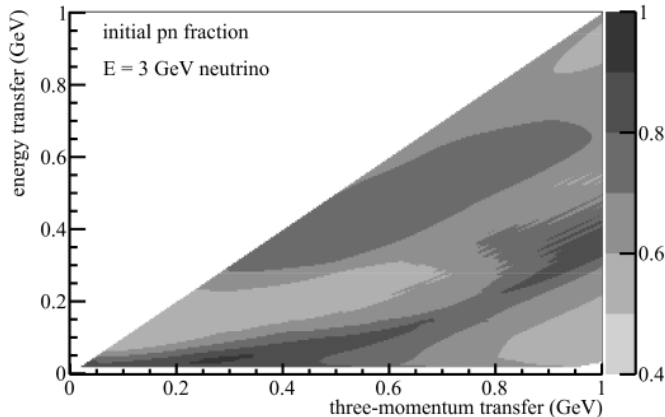


FIG. 4. The fraction of the 2p2h cross section coming from an initial $pn$ pair for 3 GeV neutrinos. The antineutrino trends are very similar. The momentum transfer axes only go to 1.0 GeV in this plot.

in the kinematic plane. In addition to the 5/6 $pn$ initial state at $\Delta$ kinematics and 50% $pn$ initial state at the non-$\Delta$ peak. There is a ridge of high $pn$ initial state just below this from the interference term and extending underneath the location of the QE peak.

Electron scattering measurements of SRC effects summarized in [20] show the initial state for the SRC process is > 90% $pn$ pairs, deduced from different types of measurements. Our model for QE does not provide a prediction for this aspect of the process. Given the charged-current nature of the interaction, a reasonable guess is the neutrino case (before hadron rescattering) would have an excess of outgoing $pp$ relative to $pn$ in which the supposed spectator nucleon shows a large momentum opposite to the initial state of its struck partner, with the antineutrino providing the same for nn pairs. This would be a different character than the low $Q^2$ 2p2h estimate presented here, though it is similar to the portion of of the 2p2h cross section with QE kinematics affected by the interference with the $\Delta$ absorption component. Overall, this model predicts a complicated isospin dependence that would vary substantially with different lepton kinematics.

### D. Variation with the size of the nucleus

The 2p2h cross section without the $\Delta$ absorption component, integrated to $q_3 = 1.2$ GeV, varies linearly with the size of an isoscalar nucleus. The 2p2h cross section

including $\Delta$ absorption shows deviations from linear dependence; $^{16}O/^{12}C = 1.5$ and $^{40}Ca/^{12}C = 4.0$, though the $\Delta$ component is expected to be nonlinear in this way. Thus, the full neutrino 2p2h cross section grows a bit faster than the number of nucleons, behavior that looks compatible with the results observed for electron scattering [22, 23].

Typical also of QE calculations with realistic nuclear models, as the nucleus size increases, the cross sections are lower at forward angles and very-low $Q^2$ and enhanced at very low energy transfer.

## IV. DISCUSSION

There are experimental data and two other models in this energy range available for initial comparisons.

### A. Super scaling approximation (SuSA)

Super scaling approximation model is a fully relativistic scheme [24] that provides a good representation of all existing QE electron scattering data for high enough momentum and energy transfers, to the extent that quasielastic scattering can be isolated. Thus, it incorporates the correct $q_3$ and $q_0$ dependence of the $(e, e')$ spectrum. The SuSA model is expected to provide a good description of $\nu$ and $\bar{\nu}$ CCQE data lacking only the two-body 2p2h contributions which will increase the QE-like cross sections. It has been recently extended up to very high neutrino energies [25] and compared to MiniBooNE and NOMAD CCQE cross sections. The SuSA model predicts cross sections that saturate with neutrino energy, like the underlying QE process, and are always lower than a Fermi gas model, the same behavior as the RPA model presented here. On the other hand, SuSA underestimates the MiniBooNE data, leaving enough room at these energies for the 2p2h contributions studied in this work.

Our RPA model was tuned to low momentum transfer data, including muon capture, and the SuSA expression of moderate momentum transfer electron scattering data is complementary. Though comparisons to just the $\sigma(E)$ cross sections are indirect, the results in Figs. 1 and 2 of [25], both absolute and relative to the Fermi gas model they present, compare well with our RPA model. The SuSA predictions fall between our default model and an artificial estimate with zero enhancement at moderate and high $q^2$. This observation suggests that the intermediate, explicitly relativistic alternate version in our paper is close to what an extrapolation of moderate $q^2$ electron scattering data would prescribe.

## B. Transverse enhancement model (TEM)

An empirical extraction of missing components of the cross section has been obtained from electron scattering data, along with a suggestion for how to approximate it in the neutrino case [26], which they refer to an enhancement of the transverse component of the cross section. This extraction of the cross section was done with inclusive electron scattering and a model that included $\Delta$ production. Under the assumption that the enhancement is coming from the 2p2h component and/or long and short-range correlations, the appropriate comparison is the version of our model which does not include the $\Delta$ absorption component.

In [26], application of the transverse enhancement to the neutrino case is to modify the $G_{Mp}$ and $G_{Mn}$ form factors as the same function of $Q^2$ that described the electron scattering data, and not change the longitudinal or axial form factors. As implemented, this insight is a function of $Q^2$ only, and does not preserve the kinematic features that fill in the dip of the electron scattering data from which it was obtained. Despite this, a prediction for the distortion of the $Q^2$ distribution is presented for a neutrino energy of 3 GeV.

At $Q^2 = 0.2, 0.5, 1.0, 2.0$ GeV$^2$ it enhances the cross section by 20%, 30%, 18%, and 5%, but the enhancement approaches zero as $Q^2$ approaches zero. Their enhancement also is constant with energy for the QE process above 2.0 GeV neutrino energy. Our 2p2h without $\Delta$ absorption model yields an enhancement of 18% and 15% for the first two data points, and in general the contribution to the cross section continues to rise from $Q^2 = 0.5$ GeV$^2$ down to zero. Because we have truncated the 2p2h model, the values and trend in the higher $Q^2$ regions cannot be compared. However, the RPA enhancement is also driven by the transverse component, and in combination with the 2p2h model might be describing the same underlying physics. In this case the magnitude and direction of the enhancement is similar, with the TEM reaching its maximum enhancement earlier in $Q^2$ than the model presented in this paper.

## C. NOMAD

The NOMAD experiment analyzed a set of QE-like interactions on carbon [27] whose flux has an average energy of 25.9 GeV for neutrino and 17.6 GeV for antineutrino. The average energy is high due to a long high energy tail. The total neutrino event rate peaks near 5 GeV, so there is a substantial portion of their event rate between 3 and 10 GeV.

They divide their data into a two-track sample which is primarily $Q^2$ above 0.3 GeV$^2$ (Fig. 14 in their paper) and also a one track sample which is primarily low $Q^2$ but includes higher $Q^2$ interactions where the proton was not reconstructed. From this they estimate how much they should enhance the QE cross section so that their

simulation describes the data, and also how to modify the axial mass parameter so the simulation describes the $Q^2$ shape of the data.

Our model produces a low $Q^2$ sample that is suppressed by the RPA effects, but some of the cross section returns with the addition of the 2p2h contribution. Quantitatively how strong this is for a NOMAD-like one-track sample depends on what fraction of the sample comes from higher $Q^2$ interactions, which is not provided. The high $Q^2$ sample is made with a selection that requires the kinematics to agree with the QE prediction with little missing momentum. This should systematically reject a large fraction of the 2p2h component, as well as QE and pion production where the hadrons rescattered as they exited the nucleus. A sample like this could be a very good place to test the effects of SRC alone. Our model predicts an overall enhancement of the cross section of around 15% and that RPA effects would give a relative deficit at $Q^2 = 0.3$ and excess at 1.5 GeV$^2$ compared to QE without RPA.

In the NOMAD analysis, a large source of uncertainty comes from their final state interaction model, which is implemented within the package DPMJET [28], a calculation developed for TeV accelerator and cosmic ray modeling of hadronic shower development. The NOMAD authors tune a "formation time" parameter $\tau_0$ to the data without considering RPA or 2p2h effects, common procedure in that era. They present results repeating their analysis with three different amounts of final state interactions, to illustrate the model agreement to the data regardless of the tuning. With more final state interactions (by decreasing $\tau_0$) the trend is to need fewer events in the one-track sample and more events in the two track sample. The lowest parameter value they tested, $\tau_0 = 0.6$ (more FSI than their favorite tune) is close to the 0.5 value they determined from their tuning procedure to be an appropriate one-sigma extreme. For this choice of parameter, their simulation underpredicts the two-track event rate by 8% but has the low-$Q^2$ one-track event rate about right. The shape fit returned a poor chis-quare and they do not show the distributions, but the other two fits were trending toward the shape distortion we describe, and their Fig. 14, with its $\tau_0$ parameter at 1.0, already shows a mild distortion in the $Q^2$ shape which is just under half of what our model suggests. A quantitative analysis cannot be done without more information about the acceptance and FSI model, and our SRC part of the model has a significant uncertainty in the $Q^2$ region of their two-track sample. However, the range of results within the context of their analysis certainly allows for the presence of substantial RPA and 2p2h effects in the data.

## D. Other data from $Q^2$ shape fits

Other high statistics experiments with substantial event rate above 1 GeV include the published result from

the K2K SciFi detector [29] and results from K2K SciBar [30] and MINOS [31] in conference proceedings. They report high fit values when extracting an axial mass $M_A$ parameter using a shape-only fit to the $Q^2$ distribution. The fundamental observation is the simulation overpredicts the relative event rate at very low $Q^2$ and underpredicts the rate at high $Q^2$. Again, effects due to RPA and 2p2h were not routinely considered at the time of those analyses, so the suggestion is a combination of high $M_A$ and additional suppression at very-low $Q^2$ could describe the data. The model presented here, with RPA providing a large $Q^2$ shape distortion and modest 2p2h contribution returning some but not all event rate at very-low $Q^2$ has the same features.

## E.   MiniBooNE and SRC

Most of the MiniBooNE data is at lower energy than we consider in this paper and comparisons with this model have already been made [7], but the effects on the $Q^2$ distribution due to RPA are the same until close to the backscattering kinematic cutoff. Data from the higher energy portion of the MiniBooNE flux produces significant event rate with $0.5 < Q^2 < 1.0$ GeV$^2$, which is where our model predicts a relatively small enhancement of the cross section due to 2p2h events but a significant enhancement from the transverse part which strongly depends on the SRC part of the RPA model. Though the SRC model is not tuned to neutrino data, the enhancement does contribute to the agreement at high $Q^2$ (and high $E_\nu$) portion of the data.

The calculation for the MiniBooNE flux is shown in Fig. 3 of Ref. [7] with and without RPA effects for one angle bin. Most of the discussion in [7] focuses on how well the combined low $Q^2$ RPA and 2p2h contributions describe the MiniBooNE double differential cross sections. In the context of the results presented here, we call attention to regions of the cross section where the SRC effects are particularly significant. The $T_\mu$ range from 1 GeV to 1.5 GeV in that figure corresponds to this range of $0.5 < Q^2 < 1.0$ GeV$^2$. The transverse part of the in-medium baryon-baryon interaction entering in the RPA effects improves the fit, though both are consistent within the errors on the data, which already include a 10% reduction of the flux described for that figure. Similarly, many of the data points in the angle bins near $\cos\theta = 0$ shown in Fig. 1 of that paper correspond to a similar region of $Q^2$ but lower muon energy. The prediction without RPA effects for those data points is consistently lower than the data by about 1.5 times the error bar, though if the 10% reduction in the flux is included both curves would be consistent with the data.

## F.   MINERvA

MINERvA's first published results [32, 33] show a distortion of the shape of the $Q^2$ spectrum qualitatively similar to other experiments; the simulation overpredicts the relative rate at low $Q^2$ and underpredicts the rate at high $Q^2$. The MINERvA data are presented as an unfolded differential cross section and a shape relative to the default QE model from the GENIE event generator. The shape comparison has uncertainties under 10% because the uncertainty in the flux substantially cancels out.

Figure 5 compares this model to the MINERvA results. The model is convoluted with the MINERvA flux between 1.5 and 10 GeV. The appropriate ratio to form for comparison to the MINERvA results in Figs. 4 of [32, 33] uses the flux weighted QE without RPA in the denominator. The QE with RPA model is shown with the default high $Q^2$ behavior (solid lines) and again with the alternate behavior (long-dashed lines) mentioned in Sec. III B.

For this comparison, the 2p2h $\Delta$ component is included; the GENIE model includes pion absorption but not an additional specific $\Delta N \to NN$ absorption process, which affects the size of their background subtraction. The $Q^2$ distribution for the 2p2h component is reconstructed from the muon kinematic quantities using the QE assumption, just as the MINERvA data and simulated samples are. The result is an additional distortion of the $Q^2$ distribution which is still pronounced at 3 GeV, boosting the 2p2h rate at reco $Q^2$ near zero by 20% and reducing it by that much at $Q^2 = 1$ GeV$^2$ compared to the true $Q^2$, but the distortion is only one-quarter that much at 10 GeV. There is no significant reco bias for the QE component implemented in this model, only some additional smearing.

The model describes absolute cross section well. The area normalized ratio, with reduced flux uncertainties is also modestly in agreement. The trend upward with increasing $Q^2$ is similar, the magnitude of the trend is too large in the default model but about right for the smaller RPA variation. Another possible interpretation, similar to the comparison with the TEM, is that the model peaks at higher $Q^2$, and more investigation into this behavior might be warranted.

The calculations presented here have not been tuned or modified for higher energy behavior except for the cut in three-momentum transfer and the alternate RPA $Q^2$ dependence. The quality of the MINERvA data and the uncertainties in the model are such that 5% to 10% sized effects are now relevant. Though detailed investigation is beyond the scope of this paper, several simple estimates of effects already mentioned do not individually make the ratios agree conclusively. This includes details specific to the MINERvA situation: considering the correlation presented in the MINERvA systematic uncertainties, energy and angle selection and unfolding effects, and importantly how much $\Delta$ component should be included in the comparison. On the model side, the QE with no
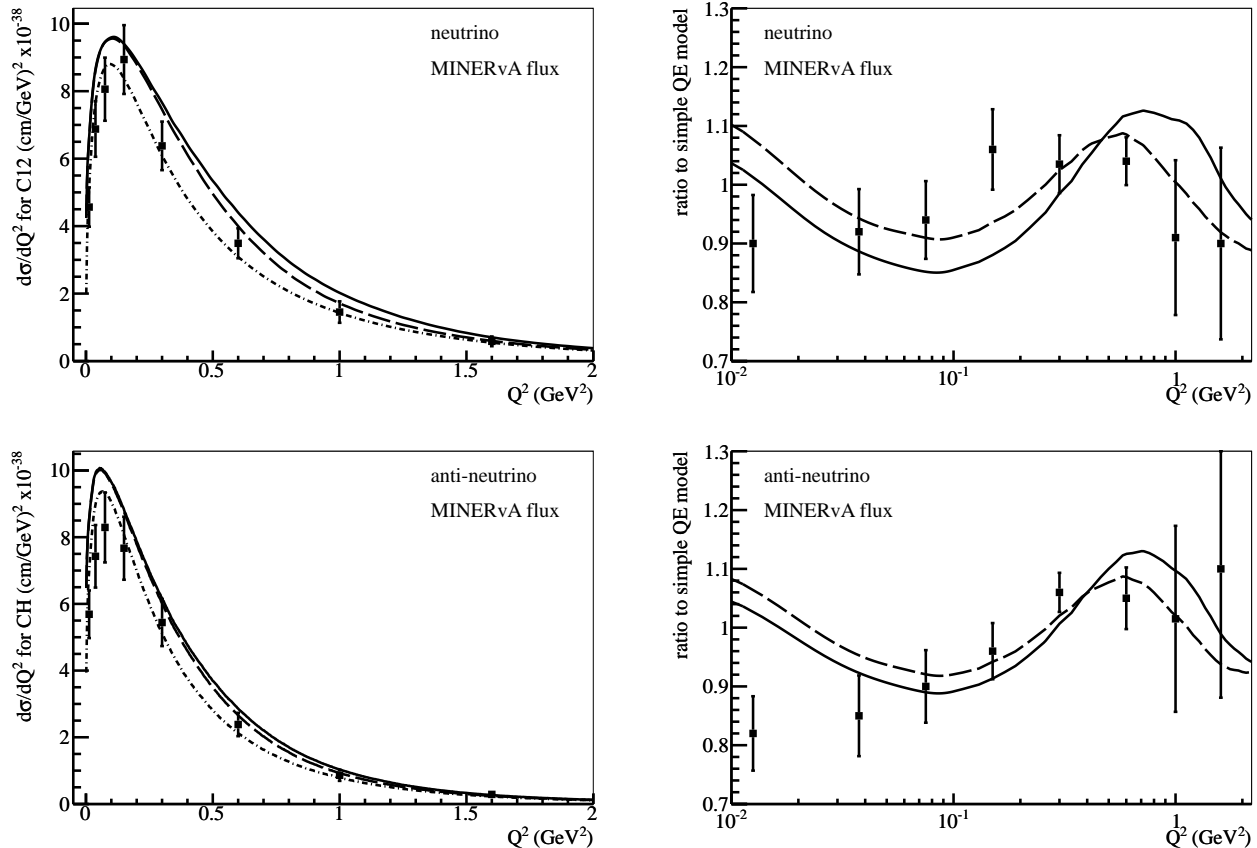
FIG. 5. Differential $Q^2$ distribution with 2p2h reconstructed from muon kinematics and QE with RPA effects and MINERvA flux (solid line) compared to MINERvA data. Neutrino (top) and antineutrino (bottom) with the ratio (right) that reduces several uncertainties especially from the flux. The flux averaged calculation without RPA and without 2p2h is shown in the absolute plot (left, dot-dashed line), and is the denominator of the calculation in the ratio plot. The ratio for the MINERvA data is directly from [32, 33], which has a flux integrated cross section from GENIE for the denominator and the area normalization. The RPA calculation with the alternate high $Q^2$ dependence is the long-dashed line.

RPA (dot-dashed line) has a different shape than GENIE by $\pm 5\%$, tuning the QE $M_A$ or form factors may be reasonable, and a simple estimate of uncertainties related to the high $Q^2$ behavior of the RPA effects are already presented.

The MINERvA results, especially Figs. 5 in [32, 33] also include the indication that there is an excess of energy carried by protons in the neutrino case, and little or no such excess of protons in the antineutrino case. Though the hadron final state kinematics are not calculated here, there are two elements that can be described roughly. The 2p2h component without the $\Delta$ is expected to lead to a $pp$ final state half the time, and $5/6$ of the time for the $\Delta$ absorption component, before additional intranuclear rescattering occurs. For the antineutrino case, these are the fractions that lead to an $nn$ final state. Compared to the pure QE process (before rescattering effects), both pick up additional protons in the final state if two nucleons leave the nucleus, and give the lead nucleon or both a little more energy than the QE process. As noted in the MINERvA papers and in

[20], the SRC process in electron scattering is dominated by the $pn$ initial state, which becomes $pp$ final state for CC neutrino scattering and $nn$ for antineutrino. Though not the case for an average over the 2p2h component of the model presented here, the portion very close to QE kinematics is predicted to similarly be enriched in the $pn$ initial state. This preferentially produces more proton energy for the neutrino case.

## V. CONCLUSION

A microscopic calculation of the neutrino and antineutrino 2p2h interaction processes without a pion in the final state produces a cross section that ranges from 26% to 29% of the QE cross section (14% to 15% for the non-$\Delta$ component) at energies from 3 and 10 GeV and for isoscalar nuclei with A $\geq$ 12. For antineutrinos, the range is from 33% to 32% for the full pionless calculation and 18% to 17% without $\Delta$ absorption. These events have a kinematic signature that is different than QE events,

they fill in the "dip" region and most would be reconstructed with systematically low neutrino energy if only lepton kinematics and the QE assumption is used. The mix of initial state for these 2p2h interactions has a complicated dependence, from 50% to 80% *pn* initial state for the non-$\Delta$ and $\Delta$ peaks, respectively, and a high near QE kinematics. The QE cross section is also significantly modified at these energies especially when RPA calculations of the effect of nuclear correlations are included. For an analysis of data describing the shape of the $Q^2$ distribution, this is likely a larger effect.

This calculation has the 2p2h and RPA effects widely believed to be relevant and present in electron scattering and also describes the low energy MiniBooNE data. Individually, these effects do not modify the simple QE model in a way that would match the data but together they qualitatively describe a distortion of the $Q^2$ spectrum that would likely lead to an anomalous value for the axial mass parameter for experiments with energies up to 10 GeV. When confronted with the MINERvA data and its small uncertainties, the model has the qualitative features and magnitude to give reasonable agreement. Fu-

ture MINERvA analyses, including higher $Q^2$ hadron and 2D muon kinematic distributions, combined with refinements of the high $Q^2$ part of this model and its application to the MINERvA situation look very promising.

[1] A. Aguilar-Arevalo *et al.* (MiniBooNE Collaboration), Phys.Rev. **D81**, 092005 (2010), arXiv:1002.2680 [hep-ex].
[2] J. G. Morfin, J. Nieves, and J. T. Sobczyk, Adv.High Energy Phys. **2012**, 934597 (2012), arXiv:1209.6586 [hep-ex].
[3] M. Martini, M. Ericson, G. Chanfray, and J. Marteau, Phys. Rev. **C80**, 065501 (2009), arXiv:0910.2622 [nucl-th].
[4] M. Martini, M. Ericson, G. Chanfray, and J. Marteau, Phys. Rev. C **81**, 045502 (2010).
[5] M. Martini, M. Ericson, and G. Chanfray, Phys. Rev. C **84**, 055502 (2011).
[6] J. Nieves, I. Ruiz Simo, and M. Vicente Vacas, Phys. Rev. **C83**, 045501 (2011), arXiv:1102.2777 [hep-ph].
[7] J. Nieves, I. Ruiz Simo, and M. Vicente Vacas, Phys.Lett. **B707**, 72 (2012), arXiv:1106.5374 [hep-ph].
[8] J. Nieves, I. R. Simo, and M. V. Vacas, Phys. Lett. **B721**, 90 (2013), arXiv:1302.0703 [hep-ph].
[9] J. Amaro, M. Barbaro, J. Caballero, T. Donnelly, and C. Williamson, Phys.Lett. **B696**, 151 (2011), arXiv:1010.1708 [nucl-th].
[10] J. Amaro, M. Barbaro, J. Caballero, and T. Donnelly, Phys. Rev. Lett. **108**, 152501 (2012), arXiv:1112.2123 [nucl-th].
[11] J. Nieves, J. E. Amaro, and M. Valverde, Phys. Rev. **C70**, 055503 (2004), arXiv:nucl-th/0408005 [nucl-th].
[12] J. Nieves, M. Valverde, and M. Vicente Vacas, Phys. Rev. **C73**, 025504 (2006), arXiv:hep-ph/0511204 [hep-ph].
[13] J. Nieves, F. Sanchez, I. Ruiz Simo, and M. Vicente Vacas, Phys. Rev. **D85**, 113008 (2012), arXiv:1204.5404 [hep-ph].
[14] S. K. Singh, N. C. Mukhopadhyay, and E. Oset, Phys. Rev. C **57**, 2687 (1998).

[15] S. Galster, H. Klein, J. Moritz, K. Schmidt, D. Wegener, *et al.*, Nucl.Phys. **B32**, 221 (1971).
[16] C. Andreopoulos *et al.*, Nucl. Instrum. Meth. **A614**, 87 (2010), arXiv:0905.2517 [hep-ph].
[17] A. Gil, J. Nieves, and E. Oset, Nucl.Phys. **A627**, 543 (1997), arXiv:nucl-th/9711009 [nucl-th].
[18] T. Leitner, O. Buss, L. Alvarez-Ruso, and U. Mosel, Phys.Rev. **C79**, 034601 (2009), arXiv:0812.0587 [nucl-th].
[19] T. J. Leitner, Ph.D. thesis, Justus-Liebig-Universitat Geissen (2009).
[20] J. Arrington, D. Higinbotham, G. Rosner, and M. Sargsian, Prog.Part.Nucl.Phys. **67**, 898 (2012), arXiv:1104.1196 [nucl-ex].
[21] O. Hen, D. Higinbotham, G. Miller, E. Piasetzky, and L. Weinstein, Int. J. Mod. Phys. E. 22, **1330017** (2013), 10.1142/S0218301313300178, arXiv:1304.2813 [nucl-th].
[22] J. Van Orden and T. Donnelly, Annals Phys. **131**, 451 (1981).
[23] A. De Pace, M. Nardi, W. Alberico, T. Donnelly, and A. Molinari, Nucl.Phys. **A741**, 249 (2004), arXiv:nucl-th/0403023 [nucl-th].
[24] J. E. Amaro, M. Barbaro, J. Caballero, T. Donnelly, A. Molinari, *et al.*, Phys.Rev. **C71**, 015501 (2005), arXiv:nucl-th/0409078 [nucl-th].
[25] G. Megias, J. Amaro, M. Barbaro, J. Caballero, and T. Donnelly, Phys.Lett. **B725**, 170 (2013), arXiv:1305.6884 [nucl-th].
[26] A. Bodek, H. Budd, and M. Christy, Eur. Phys. J. **C71**, 1726 (2011), arXiv:1106.0340 [hep-ph].
[27] V. Lyubushkin *et al.* (NOMAD Collaboration), Eur.Phys.J. **C63**, 355 (2009), arXiv:0812.4543 [hep-ex].
[28] J. Ranft, Z.Phys. **C43**, 439 (1989).
[29] R. Gran *et al.* (K2K Collaboration), Phys.Rev. **D74**,

052002 (2006), arXiv:hep-ex/0603034 [hep-ex].

[30] X. Espinal and F. Sanchez (K2K Collaboration), AIP Conf. Proc. **967**, 117 (2007), arXiv:hep-ex/0603034.

[31] M. Dorman (MINOS Collaboration), AIP Conf. Proc. **1189**, 133 (2009).

[32] L. Fields *et al.* (MINERvA Collaboration), Phys. Rev. Lett. 111, **022501** (2013), 10.1103/PhysRevLett.111.022501, arXiv:1305.2234 [hep-ex].

[33] G. Fiorentini *et al.* (MINERvA Collaboration), Phys. Rev. Lett. 111, **022502** (2013), 10.1103/PhysRevLett.111.022502, arXiv:1305.2243 [hep-ex].